Eur. Phys. J. A **28**, s01, 81–90 (2006)
DOI: 10.1140/epja/i2006-09-009-2

EPJ A direct
electronic only

Electromagnetic form factors of the nucleon

Experiments at MAMI

M. Ostrick[a]

Physikalisches Institut, Universität Bonn, 55115 Bonn, Germany

/
Published online: 12 May 2006 –

Abstract. Elastic form factors are of fundamental importance for the understanding of microscopic spatial structures. In case of the proton and the neutron, charge and magnetic form factors can be studied in elastic electron scattering. Techniques to accelerate polarised continuous electron beams, the availability of polarised targets as well as modern concepts and instrumentation for coincidence experiments and recoil polarimetry had an enormous impact on these measurements. The developments and experiments at the Mainz Microtron MAMI will be discussed in a general context.

PACS. 13.40.Gp Electromagnetic form factors – 13.85.Dz Elastic scattering – 13.88.+e Polarization in interactions and scattering – 25.30.Bf Elastic electron scattering

1 Introduction

Elastic and inelastic scattering experiments at different energy scales and with different projectiles provide essential insight into microscopic structures in terms of excitation spectra or spatial and momentum distributions of constituents.

Form factors measured in elastic scattering are in particular determined by the ability of a system to absorb a momentum without excitation and, therefore, reflects the wave function of constituents in the ground state. Nonrelativistically, elastic form factors are momentum representations of spatial densities like mass or electroweak charge densities. In case of spherical symmetry, an expansion close to the static limit of zero momentum transfer is given by the integral quantity, *e.g.* the total charge Z, and the corresponding mean square radius:

$$F(|\vec{q}\,|) = Z - \frac{q^2}{6}\left\langle r^2\right\rangle + O(q^4). \tag{1}$$

The first evidence for such finite size effects of atomic nuclei was found by Lyman, Hanson and Scott in electron scattering experiments at a 20 MeV betatron [1]. Their pioneering work together with the first electron-proton-scattering experiments by Hofstadter [2] mark the beginning of a fruitful era of using electromagnetic probes to analyse nuclear and subnuclear hadronic structures. The electromagnetic coupling is weak enough to allow a perturbative treatment and strong enough for precise measurements even at higher values of momentum transfer.

Compared to pointlike fermions, the contributions of charge and total magnetic moment to the vector current of protons and neutrons are modified by charge ($G_{E,p}, G_{E,n}$) and magnetic form factors ($G_{M,p}, G_{M,n}$) which depend on the square of the 4–momentum transfer Q^2.

The unpolarised cross section for electron scattering off nucleons can be expressed in leading order as an incoherent sum of the response to longitudinal and transverse polarisation components of the exchanged virtual photon. In case of elastic scattering these responses are equal to $G_E^2(Q^2)$ and $\tau G_M^2(Q^2)$, respectively:

$$\frac{\mathrm{d}\sigma}{\mathrm{d}\Omega} = \frac{\sigma_M}{\epsilon(1+\tau)}\left(\epsilon G_E^2(Q^2) + \tau G_M^2(Q^2)\right). \tag{2}$$

Here $\tau = Q^2/4M^2$, $\epsilon = [1 + 2(1+\tau)\tan^2\frac{\vartheta_e}{2}]^{-1}$ describes the photon polarisation and σ_M is the Mott cross section for a pointlike particle. In principle, both form factors can thus be determined by studying the ϵ dependence of the cross section at fixed values of Q^2. This technique, known as Rosenbluth or LT separation, has been intensively used in single arm experiments at low duty cycle machines. It requires measurements at different scattering angles and beam energies as well as the knowledge of absolute luminosities. This Rosenbluth separation technique is intrinsically limited if one of the two summands in the unpolarised cross section, G_E^2 or τG_M^2, is small compared to the other one. In this case, only the dominating form factor can be extracted reliably.

For the proton, since two decades the cross section measurements of Simon *et al.* at the Mainz 300 MeV–Linac provide the most precise data for $G_{E,p}$ at low Q^2 allowing an accurate determination of the proton charge radius [3]. However, at higher values of Q^2 the transverse part, $\sigma_T \sim \tau G_M^2$, is getting more and more dominant and a separation of $G_{E,p}$ suffers from statistical as well as

[a] e-mail: ostrick@kph.uni-mainz.de

from systematic uncertainties. In single-arm experiments at high momentum transfer up to $Q^2 = 30\,\mathrm{GeV}^2$ only the proton magnetic form factor, $G_{M,p}$, has been determined precisely at the SLAC accelerator [4].

Measurements of neutron form factors, $G_{M,n}$ and $G_{E,n}$, are even more difficult due to the lack of a free neutron target and the smallness of $G_{E,n}$ (see sect. 4.3).

The results of these unpolarised, single-arm electron scattering experiments have usually been summarised in the past in terms of the approximate scaling relation

$$G_{E,p} \approx G_{M,p}/\mu_p \approx G_{M,n}/\mu_n \tag{3}$$

and the approximate dipole form

$$G_{M,p} \approx \mu_p G_D = \left(\frac{1}{1+Q^2/m^2}\right)^2 \tag{4}$$

with the phenomenological parameter $m^2 = 0.71\,\mathrm{GeV}^2$.

Indispensable prerequisites for more detailed analyses and interpretations are precise measurements of all four nucleon form factors over a larger range in momentum transfer. To overcome the intrinsic limitations discussed above, techniques are required to accelerate polarised continuous electron beams together with polarised targets and an experimental instrumentation for coincidence experiments and recoil polarimetry. These technological and conceptual developments allow to exploit the full potential of electromagnetic probes and are characteristic for the modern era of electron scattering.

These developments and form factor measurements at the Mainz Microtron MAMI will be discussed in the next sections. A recent review on form factors and their measurements in general can be found in [5].

2 Coincidence experiments to measure $G_{M,n}$

Lacking a free neutron target Ehrenberg and Hofstadter for the first time used inclusive electron scattering off light nuclei in quasi free kinematics to measure the neutron magnetic form factor [6].

In general, this procedure requires a separation of the longitudinal $R_L \sim G_{E,p}^2 + G_{E,n}^2$ and the transverse cross section $R_T \sim G_{M,p}^2 + G_{M,n}^2$ and a subsequent subtraction of the proton contribution. In addition to this complex procedure the influence of nuclear binding introduces model dependences even in case of the deuteron. At momentum transfers above 1–2 $(\mathrm{GeV}/c)^2$ the effect of $G_{M,n}$ is large enough to employ this technique reliably [7].

The subtraction of the substantial proton contribution can be avoided by measuring the scattered neutron in coincidence with the electron [8]. In order to achieve acceptable signal-to-noise ratios in such coincidence experiments, electron beams with a high duty factor are essential. The difficulty is then shifted to the experimental task to calibrate and monitor the neutron detection efficiency. In addition, the sensitivity to nuclear structure can be significantly reduced by measuring the cross section ratio

$$R_d = \frac{\sigma\left(d(e,e'n)\right)}{\sigma\left(d(e,e'p)\right)} \tag{5}$$

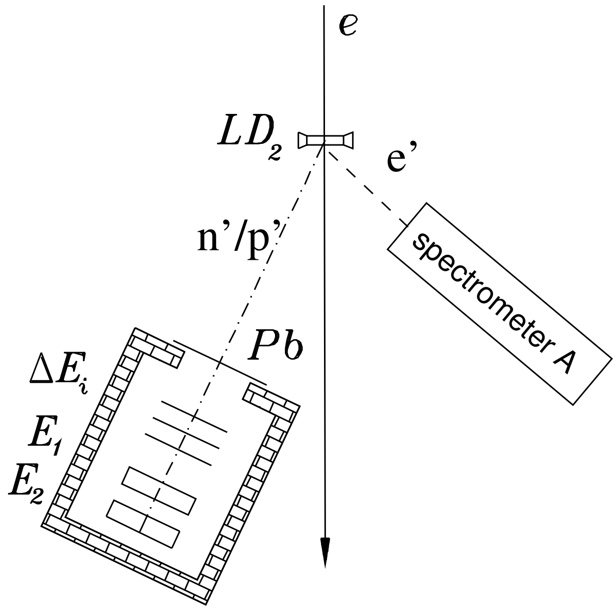

Fig. 1. Setup to measure R_d at MAMI.

for scattering from neutrons and protons in quasi-free kinematics. In plane-wave-impulse-approximation spectral functions and the elementary electron nucleon scattering factorise so that the dependence on nuclear wave functions cancels in the ratio. Higher-order corrections like final state interactions (FSI) or meson exchange currents (MEC) are small ($\sim 2\%$) and calculable [9,10].

Measurements of the ratio R_d thus provided a significant break-through in the knowledge of $G_{M,n}$ at low Q^2 and have been pioneered at NIKHEF [11], ELSA [12] and MAMI [13,14].

The setup at MAMI is shown in fig. 1. The electrons are detected in a magnetic spectrometer with a solid angle of 28 msr, a momentum acceptance of 20% and a resolution $\Delta p/p \leq 10^{-4}$ (spectrometer A [15]). In coincidence with the electron, the scattered nucleons are identified as proton or neutron in a well shielded scintillator array. As $d(e,e'n)$ and $d(e,e'p)$ yields are measured simultaneously, the ratio R_d is independent of fluctuations in luminosity and acceptance of the electron detector. The main experimental difficulty is the absolute calibration and monitoring of the neutron detection efficiency which enters directly in the ratio R_d. A calibration using the kinematically complete $p(n,p)n$ reaction to tag neutrons requires measurements under different experimental conditions at a facility providing intense neutron beams (*e.g.* [16]). Considerable care has to be taken to monitor effective detection thresholds and to ensure portability of the measured efficiencies [13,14]. In contrast, Bruins *et al.* [12] used the $p(\gamma,\pi^+n)$ to calibrate their neutron detector *in situ*. However, reactions from electroproduction $p(e,\pi^+n)e'$, where the exact kinematical correlation is lost in the 3 body final state, may lead to an underestimation of the detection efficiency. This has been suggested [17,18] as origin of the 10% discrepancy in the extracted values for $G_{M,n}$ which

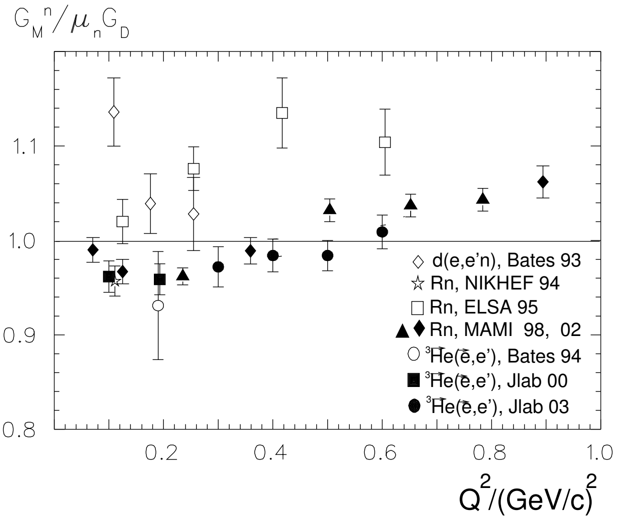

Fig. 2. The neutron magnetic form factor in units of $\mu_n G_D$ as function of Q^2 measured in coincidence and polarisation experiments [8,11,12,13,14,19,20,21].

are summarised in fig. 2 in units of the empirical dipole expression (eq. (3)).

An alternative method to determine $G_{M,n}$ is provided by inclusive scattering of polarised electrons from polarised ^{3}He in quasi-elastic kinematics [19,20,21]. Results obtained with this technique at Bates and Jefferson Lab are included in fig. 2 as well as absolute $d(e,e'n)$ cross section measurements from Bates [8].

Recently, new measurements of R_d at Q^2 values up to 5 $(\mathrm{GeV}/c)^2$ have been completed at Jefferson Lab [22]. The large solid angle covered by the CLAS spectrometer allows to perform the efficiency determination simultaneously with the R_d measurement by tagging neutrons in the $p(e,e'\pi^+)n$ reaction where both, scattered electron and π^+ are detected. Preliminary results show, that $G_{M,n}$ follows the dipole approximation up to $Q^2 = 5$ $(\mathrm{GeV}/c)^2$ within 10%.

3 Double-polarisation observables

Experiments using polarised electron beams in combination with polarised nucleons either in the initial or final state offer possibilities to measure interferences between longitudinal and transverse amplitudes which do not appear in the unpolarised cross section. This is particularly interesting in cases where one part is completely dominating and unpolarised cross section measurements are not sufficient to separate additional small amplitudes. Furthermore, most polarisation observables are insensitive to absolute luminosities and other experimental calibration factors.

In electron-neutron scattering for example, the smallness of the electric form factor $G_{E,n}$ compared to the dominant magnetic form factor makes a reliable Rosenbluth separation impossible. As mentioned above, the situation is similar for protons at high momentum transfer

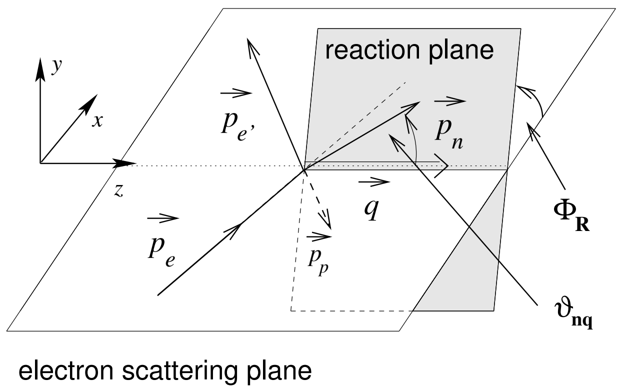

Fig. 3. Reference frame and kinematics of the $d(e,e'n)$ reaction.

where the contribution of $G_{E,p}$ to the unpolarised cross section is kinematically suppressed. The increased sensitivity of double polarisation observables to $G_{E,n}$ and $G_{E,p}$ at high Q^2 has already been pointed out more than 40 years ago [23,24,25].

For the ideal case of scattering longitudinally polarised electron off free nucleons, $N(\vec{e},e'\vec{N})$, the components of the recoil polarisation are given by

$$P_x = -P_e \frac{\sqrt{2\tau\epsilon(1-\epsilon)}\; G_E G_M}{\epsilon\, G_E^2 + \tau\, G_M^2}\,, \tag{6}$$

$$P_y = 0\,, \tag{7}$$

$$P_z = P_e \frac{\sqrt{1-\epsilon^2}\;\tau\, G_M^2}{\epsilon\, G_E^2 + \tau\, G_M^2}\,. \tag{8}$$

They are equivalent to cross section asymmetries with respect to the beam helicity for the different nucleon spin orientations in the scattering from polarised targets:

$$A_x = P_x; \quad A_y = 0; \quad A_z = -P_z. \tag{9}$$

The $\hat{x}$ and $\hat{z}$ direction are defined by the electron scattering plane with $\hat{z}$ given by the momentum transfer $\vec{q}$ (see fig. 3).

In P_x and A_x both form factors enter linearly which increases the sensitivity compared to the unpolarised cross section, if $G_E^2 \ll \tau G_M^2$.

In case of the neutron, the free e-n scattering has again to be approximated by the quasi-free scattering off light nuclei (^{2}H, ^{3}He) and one has to pay attention to nuclear binding and rescattering effects. In leading order, spectral functions cancel in the polarisation and asymmetry components being ratios of cross sections. However, higher order effects like FSI and MEC as well as influences of Fermi-motion on the projections of polarisation components have to be taken into account.

Polarised ^{3}He can be used as an effective polarised neutron target because in its ground state the two protons are dominantly in the s-state with the spins coupled to zero. Thus the spin of the ^{3}He is predominantly carried by the neutron. Additional d-wave components, meson exchange currents and final state interactions have recently been

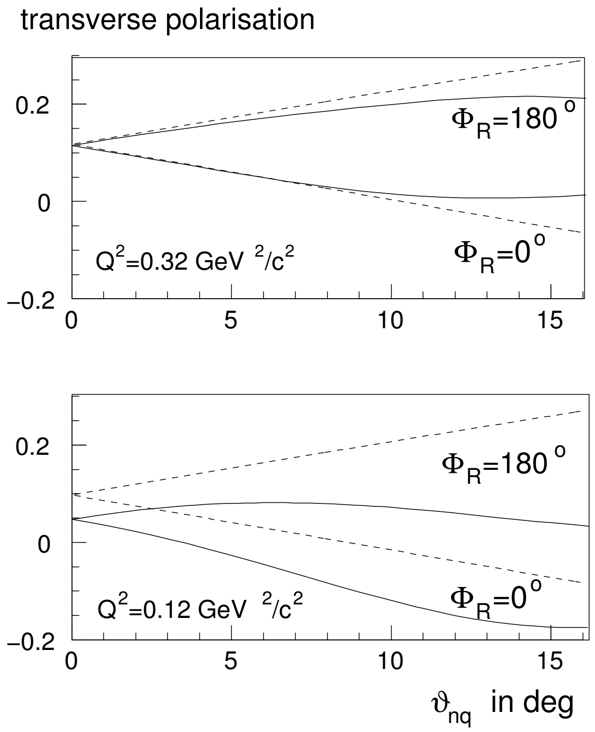

Fig. 4. Dependence of transverse neutron polarisation in the $d(\vec{e}, e'\vec{n})$ reaction on the neutron kinematics for two different values of Q^2. ϑ_{nq} is the angle between the neutron recoil momentum and momentum transfer. The dashed curves indicate the influence of the Fermi-motion, the solid curves are results of a calculation by Arenhövel [27,28] including FSI and further higher-order contributions.

analysed at low Q^2 within full three body calculations [26]. The dominant correction, that has to be applied in analyses of $^3\vec{\mathrm{H}}\mathrm{e}(\vec{e}, e'n)$ experiments, originates from scattering off protons followed by a charge-exchange reaction simulating quasifree $n(e, e'n)$ events (see sect. 4.3).

In the $d(\vec{e}, e'\vec{n})$ reaction, the neutron recoil momentum $\vec{p}_n$ in general deviates from the direction of momentum transfer $\hat{q}$ due to Fermi motion as indicated by the angles ϑ_{nq} and Φ_R in fig. 3. At finite angles ϑ_{nq} the transverse polarisation P_t of the recoiling neutron gets admixtures from the P_z component. This is demonstrated in fig. 4, where P_t is plotted as a function of the angle ϑ_{nq} for the two extreme situations $\Phi_R = 0°$ and $\Phi_R = 180°$. The dashed curves indicate the admixture of P_z due to this purely kinematical effect which averages out if the detector acceptance is completely symmetric in Φ_R.

In studying the details of the $d(\vec{e}, e'\vec{n})$ reaction, Arenhövel *et al.* have shown that meson exchange and isobar currents have a negligible effect in quasifree kinematics as does the choice of the NN-potential so that there is essentially no dependence on the deuteron wave function [27,28]. However, at momentum transfers below $Q^2 = 0.25$ $(\mathrm{GeV}/c)^2$ a strongly rising influence of final state interactions, especially of charge exchange reactions, is found (solid curves in fig. 4). This leads to a shift in the observed polarisation component P_x even in the case $\vartheta_{nq} = 0$ and has to be taken into account in the determination of $G_{E,n}$ (see section 4.3).

4 Double-polarisation experiments

The realisation of double-polarisation experiments described in the previous section demands the technically sophisticated combination of continuous, high intensity, polarised electron beams with polarised targets or recoil polarimetry. At MAMI such experiments have been performed since the beginning of the 1990s.

4.1 Polarised electrons at MAMI

In 1992 a spin-polarised electron beam was accelerated through MAMI for the first time. The electron source was based on photoemission of GaAsP illuminated by circularly polarised laser light [29]. The helicity sign of the laser and consequently of the electron beam was flipped at a rate of 1 Hz by reversing the high voltage of a Pockels cell. In order to have longitudinally polarised electrons at the experiment the spin precession in the magnetic fields of accelerator and transfer beamlines has to be compensated. As there are no depolarising resonances in a microtron, this can be done at low energies before accelerator injection or by slightly tuning the beam energy [30,31]. In the beginning, a polarisation of about 30-35% at beam currents of 5-10 μA has been achieved. The use of strained layer GaAs cathodes increased the polarisation significantly [32]. The lower quantum efficiency could be compensated by increasing the laser power and the transfer efficiency into the accelerator.

The beam polarisation is measured and monitored using the spin dependence of Mott–, Moeller– and Compton–scattering.

Today, high intensity (up to 80 μA), highly polarised ($P_e \sim 80\%$) beams with sophisticated monitoring systems are available which allow to measure even tiny parity-violating asymmetries [33,34].

4.2 Polarisation transfer to protons

In one of the early double polarisation experiments at MAMI the spin transfer to protons in the $p(\vec{e}, e'\vec{p})$ and $d(\vec{e}, e'\vec{p})$ reactions has been analysed for the first time [35]. The transverse polarisation component P_x (eq. (7)) is accessible experimentally by measuring an asymmetry in the azimuthal angular distribution (Φ') of protons scattered in a carbon analyser:

$$A(\Phi') = a_T \cdot \sin \Phi' = P_e \cdot \mathcal{A}_{\mathrm{pC}} \cdot P_x \cdot \sin \Phi'. \qquad (10)$$

The analysing power $\mathcal{A}_{\mathrm{pC}}$ of inclusive proton-carbon scattering is known and has frequently been used for spin analyses at proton facilities. With the number of events $N^{\pm}(\Phi')$ for both helicity states of the electron beam, this

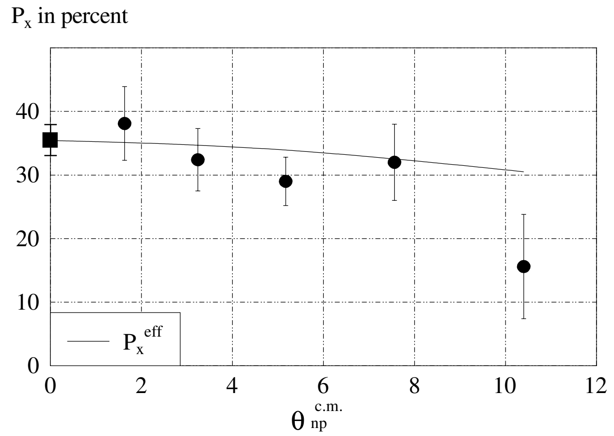

Fig. 5. Transverse proton polarisation P_x measured in $p(\vec{e},e'\vec{p})$ (square) and $d(\vec{e},e'\vec{p})$ (circles) at $Q^2 = 0.3\ (\mathrm{GeV}/c)^2$ [35]. In case of the deuteron target the observed dependence on the angle θ_{np} of the proton-neutron relative momentum is shown. The line is a calculation of Arenhövel *et al.* [27,28].

azimuthal asymmetry $A(\Phi')$ can be determined through the ratio

$$\frac{1-A(\Phi')}{1+A(\Phi')} = \sqrt{\frac{N^+(\Phi')\cdot N^-(\Phi'+\pi)}{N^-(\Phi')\cdot N^+(\Phi'+\pi)}}\,, \tag{11}$$

which is insensitive to detector efficiencies and luminosity fluctuations.

The detector system was completely non magnetic consisting out of a segmented lead-glass calorimeter for the electrons and a scintillator hodoscope including the carbon analyser for the proton detection and spin analysis.

In the kinematics chosen for the experiment the dependence of P_x on $G_{E,p}$ is weak and influences of binding and rescattering effects can be tested. The measured polarisation transfer P_x at $Q^2 = 0.3\ (\mathrm{GeV}/c)^2$ is shown in fig. 5. No significant difference in the spin transfer between free protons and protons bound in deuterons was observed at $Q^2 = 0.3\ (\mathrm{GeV}/c)^2$ in quasifree kinematics. In case of the deuteron target the results are in agreement with calculations of Arenhövel *et al.* [27,28].

The full power of measuring the polarisation transfer to protons has been demonstrated in experiments using polarimeters consisting out of tracking detectors in front and behind a carbon analyser sitting in the focal plane of a magnetic spectrometer. If the spin precession along the proton path is accurately taken into account, in principle all three polarisation components of the recoiling proton are accessible.

In case of elastic scattering the ratio P_x/P_z is directly proportional to the ratio of the charge and magnetic form factors:

$$\frac{P_x}{P_z} = \frac{\sqrt{2\epsilon}}{\sqrt{\tau(1+\epsilon)}}\cdot\frac{G_E}{G_M}\,. \tag{12}$$

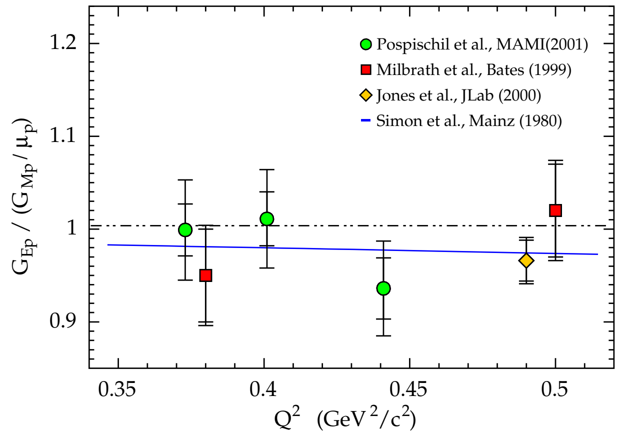

Fig. 6. The ratio $\mu_p G_{E,p}/G_{M,p}$ from polarisation transfer measurements at low Q^2 [36,37,38]. The dotted line corresponds to the exact scaling behaviour of eq. (4), the solid line is a fit to Rosenbluth separated data [3].

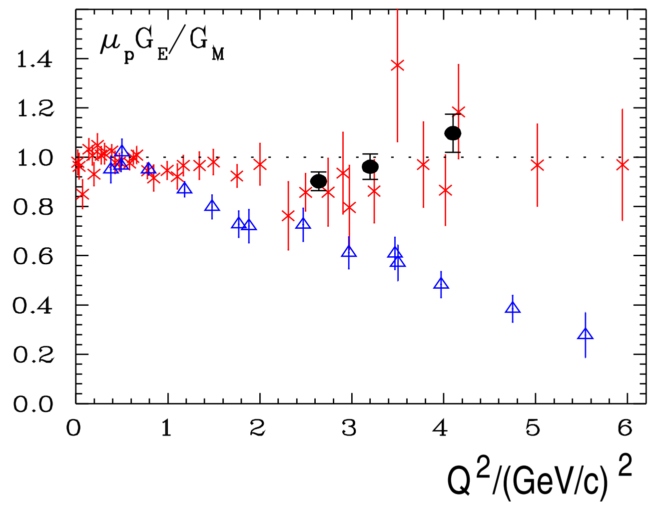

Fig. 7. The ratio $\mu_p G_{E,p}/G_{M,p}$ from polarisation transfer measurements (triangles, [38,39]) compared to results extracted from Rosenbluth separation [40,41].

Experimental calibration factors as the absolute value of the beam polarisation or the effective analysing power of the polarimeter cancel in this ratio.

The proton charge form factor has been measured using this technique at Bates [36] and MAMI [37] at low Q^2 (fig. 6) as well as in Hall A at Jefferson Lab [38,39] (fig. 7). The measurements at JLab covered a Q^2 range from 0.5 to 5 $(\mathrm{GeV}/c)^2$ and enormously influenced our knowledge about $G_{E,p}$. The observed linear decrease of the ratio $\mu_p G_{E,p}/G_{M,p}$ at $Q^2 > 1\ (\mathrm{GeV}/c)^2$ contradicts the previously assumed approximate scaling behaviour (eq. (4)) and is in clear disagreement with the results obtained by LT separations of unpolarised cross sections.

An experimental origin of this discrepancy has recently been excluded by a new dedicated Rosenbluth extraction which is in agreement with the earlier results [41]. The effect of $G_{E,p}$ in the cross section is so small, that unknown ϵ dependent corrections to the one-photon exchange approximation may have a similar size and could disturb the Rosenbluth extraction. In general, two-photon exchanges are suppressed by the electromagnetic coupling $\alpha_{em} \approx 1/137$ and they are partly taken into account in radiative corrections [42]. However, there exist contributions which depend on the hadronic structure and on intermediate excited states of the nucleon. Calculations of these corrections are model dependent and they have been neglected in the past. A recent discussion of two-photon effects and the hadronic physics involved can be found in [43].

4.3 Measurements of $G_{E,n}/G_{M,n}$

The vanishing charge of the neutron makes any small electric interaction enormously difficult to detect. Attempts to measure first moments of a charge distribution originate in the idea of Fermi and Marshal to study the scattering of thermal neutrons off atomic electrons [44]. These experiments have been refined and a negative mean square charge radius close to the so called Foldy term $3\kappa/2M_n^2 = -0.126\,\mathrm{fm}^2$ has been established [45,46]. However, a precise determination is still suffering from systematic uncertainties due to the dominating nuclear scattering amplitude [47,48].

At $Q^2 > 0$ the smallness of $G_{E,n}^2$ compared to $\tau G_{M,n}^2$ makes a reliable Rosenbluth separation impossible. Finite values for $G_{E,n}$ have been extracted from the deuteron structure function $A(Q^2)$, measured in elastic electron-deuteron scattering. $A(Q^2)$ provides sensitivity to $G_{E,n}$ through the mixed term $G_{E,p} \cdot G_{E,n}$ in the square of the isoscalar form factor $(G_{E,n} + G_{E,p})^2$. However, the necessary unfolding of the deuteron wave function introduces substantial model dependences ([49,50] and fig. 10).

The first $^3\overrightarrow{\mathrm{H}}\mathrm{e}(\overrightarrow{e}, e'n)pp$ and $D(\overrightarrow{e}, e'\overrightarrow{n})p$ experiments at MAMI have been performed with one common large solid angle detector system (fig. 8) [51,52,53,54]. The scattered electrons were detected in a segmented lead-glass calorimeter with an energy resolution $\delta E/E \sim 25\%$ sufficient to suppress inelastic events from π-production. Only the electron angles entered the reconstruction of the 3-body final state, which became kinematically complete through the measurement of the neutron time of flight and hit position in arrays of plastic scintillators well shielded by concrete and lead.

In the $d(\overrightarrow{e}, e'\overrightarrow{n})$ reaction, the polarisation of the recoiling neutron perpendicular to its momentum can be analysed using the detection process itself. n-p-scattering as well as inelastic processes, *e.g.*, $^{12}\mathrm{C}(n, n'p)^{11}\mathrm{B}$, which contribute to a neutron detection in a plastic scintillator, provide reasonable analysing power $\mathcal{A}_{\mathrm{eff}}(\Theta'_n, T_n)$. The resulting asymmetry in the azimuthal angular distribution, $N(\Phi')$, of the detected neutrons can be observed through the hit distribution in a second scintillator wall (fig. 8) and analysed via eq. (11).

In front of the analyser a dipole magnet has been installed which allows to avoid an external calibration of the effective analysing power through a controlled precession

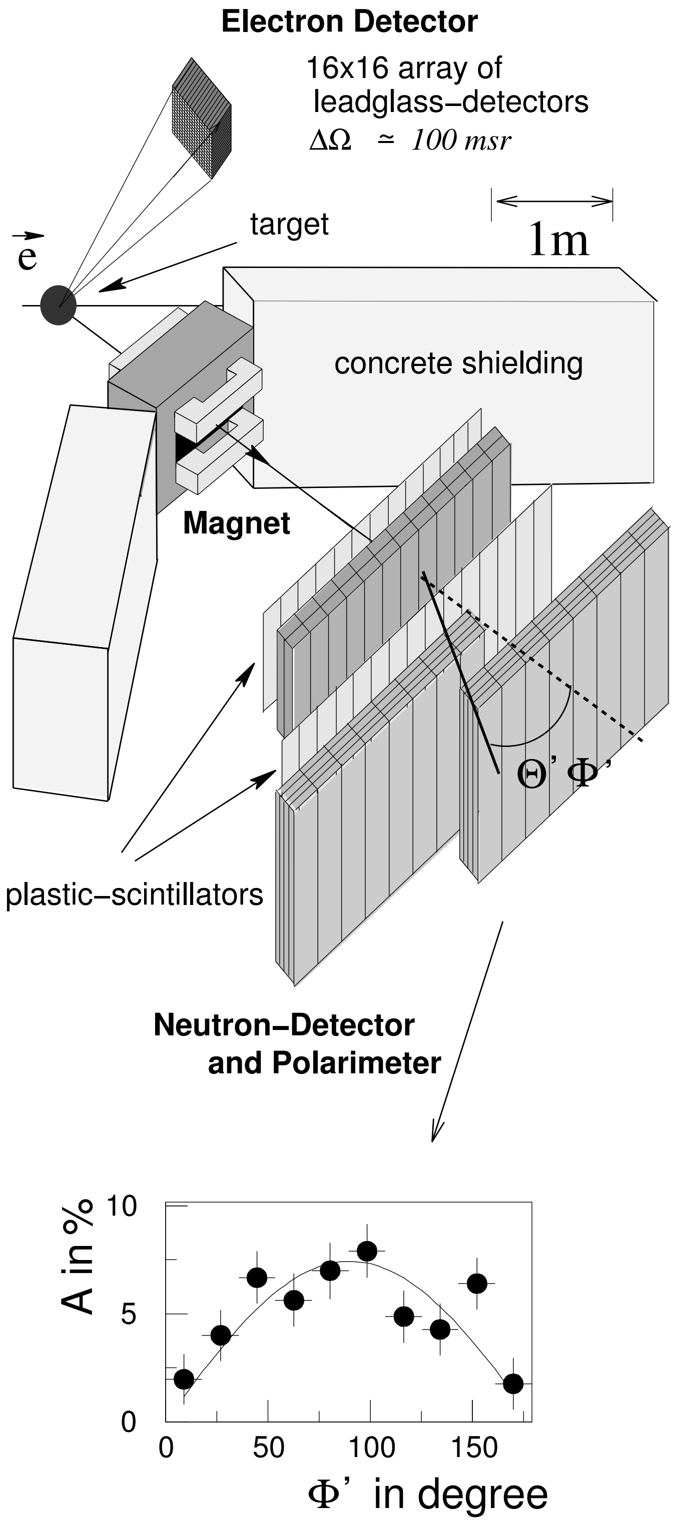

Fig. 8. Detector-setup for the first double polarisaton experiments at MAMI and a typical asymmetry in the azimuthal angular distribution of neutrons detected in both scintillator walls calculated via eq. (11).

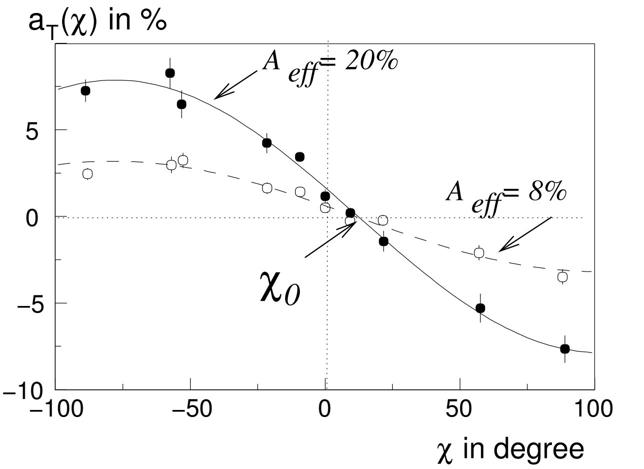

Fig. 9. Measured azimuthal asymmetries $a_\perp(\chi)$ for various precession angles χ with two different cuts on the analysing reaction leading to different analysing powers but leaving χ_0 unchanged.

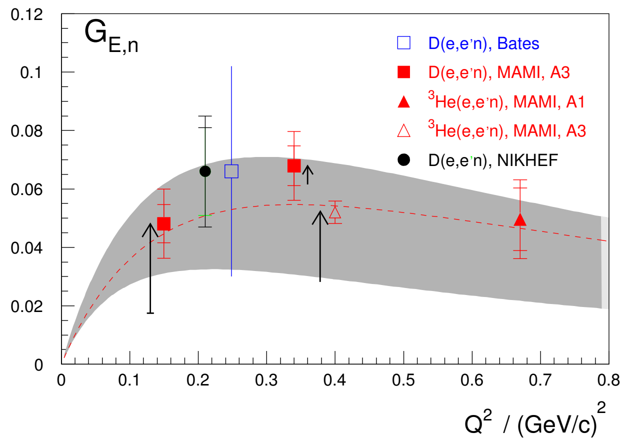

Fig. 10. First $G_{E,n}$ results from double-polarisation observables. The arrows indicate the influence of few-body effects mainly due to final state interactions. The shaded area represents the model dependence of $G_{E,n}$ values extracted from elastic $D(e,e')$ experiments [50] The dashed line is the parametrisation of Galster *et al.* [49].

of the neutron spin. This technique has become standard in modern neutron polarimeters.

After precession by the angle

$$\chi = \frac{\mu_n}{2\,\beta_n\,c} \cdot \int_L B(l)\mathrm{d}l \tag{13}$$

the transverse neutron polarisation as well as the resulting azimuthal asymmetry $a_\perp$ become a superposition of x and z components:

$$\begin{aligned} a_\perp(\chi) &= P_e \mathcal{A}_{\text{eff}}\,(P_x \cos\chi - P_z \sin\chi) \\ &= a_0 \cdot \sin(\chi - \chi_0). \end{aligned} \tag{14}$$

One immediately finds that the angle χ_0 of the zero crossing $a_\perp(\chi_0) = 0$ is directly related to the ratio P_x/P_z (eq. (12)) and depends neither on the analysing power of the polarimeter nor on the polarisation of the electron beam,

$$\tan\chi_0 = \frac{P_e \mathcal{A}_{\text{eff}}}{P_e \mathcal{A}_{\text{eff}}} \cdot \frac{P_x}{P_z}\,. \tag{15}$$

Measured asymmetries for various precession angles χ are shown in fig. 9. Kinematic cuts on the analysing reaction change the amplitude, *i.e.* the effective analysing power, but not the zero crossing angle χ_0.

To extract values for $G_{E,n}$ binding effects mainly due to final state interactions have been taken into account according to calculations of H. Arenhövel [27,28]. At low momentum transfer ($Q^2 = 0.12$ (GeV$/c)^2$) a correction of almost 100% is required which drops rapidly to 8% at $Q^2 = 0.35$ (GeV$/c)^2$ (see fig. 4, [54]).

In case of the $^3\vec{\mathrm{H}}\mathrm{e}(\vec{e}, e'n)$ reaction the ^{3}He gas is polarised by optical pumping a metastable excited state which then transfers the polarisation to the ground state. In the first experiments, after optical pumping, the gas was compressed to 1bar in the target cell [51,52]. Today typical target polarisations of about 50% at pressures up to 5 bar are achieved [55]. For different orientations of the target spin cross section asymmetries with respect to the beam helicity are measured. The arrays of plastic scintillators serve in this case as neutron detector and time of flight spectrometer only, not as polarimeter.

In 1998 no full 3 body calculations were available and the first $^3\vec{\mathrm{H}}\mathrm{e}(\vec{e}, e'n)$ experiments have been analysed under the assumption of quasifree scattering from a neutron with no higher order effects taken into account [51,52]. The initial 50% discrepancy between $d(\vec{e}, e'\vec{n})$ and $^3\vec{\mathrm{H}}\mathrm{e}(\vec{e}, e'n)$ experiments around $Q^2 = 0.3$ (GeV$/c)^2$ has been resolved in full 3-body calculations of the $^3\vec{\mathrm{H}}\mathrm{e}(\vec{e}, e'n)$ reaction including final state interactions [26]. At higher Q^2, binding and rescattering effects are expected to decrease significantly as for deuterium [55]. A detailed discussion of polarised ^{3}He–targets and their use in experiments at MAMI can be found in [56].

Figure 10 summarises results for $G_{E,n}$ obtained in the first double-polarisation experiments. The arrows indicate the necessary corrections due to final state interactions.

In the meantime, $\vec{d}(\vec{e}, e'n)$, $d(\vec{e}, e'\vec{n})$ and $^3\vec{\mathrm{H}}\mathrm{e}(\vec{e}, e'n)$ reactions have been measured several times with refined techniques. At MAMI the use of magnetic spectrometers to detect the scattered electron improved background suppression and kinematical reconstruction considerably [57,55,58]. In particular, the direction of the momentum transfer vector $\vec{q}$, which defines the relevant coordinate system for the spin analysis, can be reconstructed precisely. At Jefferson Lab the Q^2 range has been extended up to 1.5 (GeV$/c)^2$ [59,60]. Below $Q^2 = 1$ (GeV$/c)^2$, new preliminary data obtained with the Blast-detector at Bates have recently been shown [61].

Furthermore, $G_{E,n}$ has been extracted from an analysis of the deuteron quadrupole form factor F_Q obtained from recent tensor polarisation measurements in elastic electron deuteron scattering [62]. Compared to the

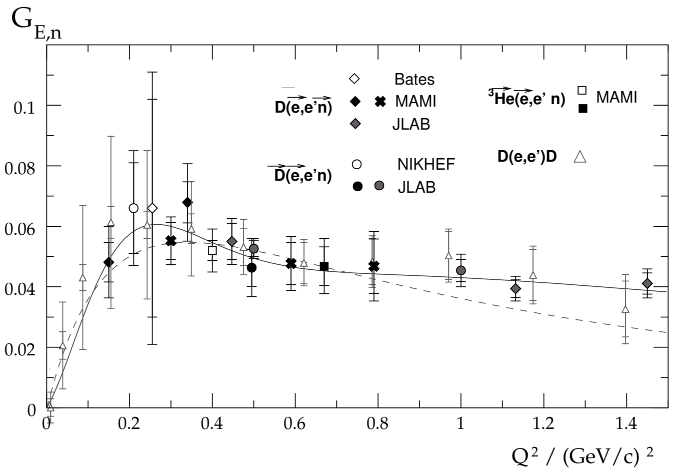

Fig. 11. Present status of $G_{E,n}$ measurements compared to the parametrisation of Galster *et al.* ([49], dashed line) and Friedrich, Walcher ([63], solid line). The data are from experiments using polarised Deuterium [64,65,59], polarised ^{3}He [55, 26,58], recoil polarisation [66,54,60], and from an analysis of the elastic deuteron quadrupole form factor [62].

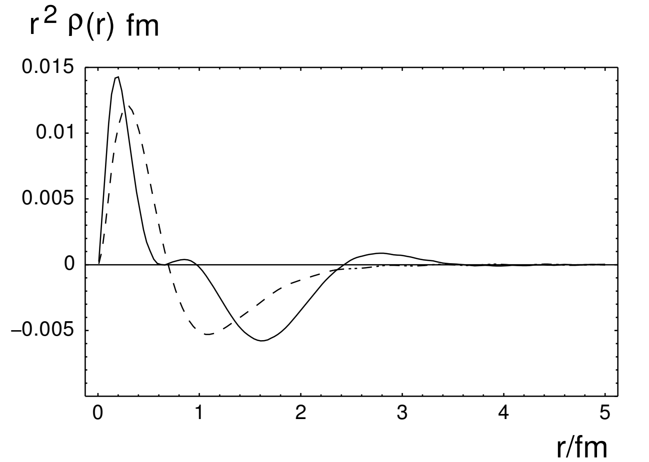

Fig. 12. Neutron charge distribution obtained from Fourier transforms of $G_{E,n}$ by Friedrich and Walcher (solid line [63]) and the Galster parametrisation (dashed line).

above-mentioned older analyses of the elastic deuteron structure functions A [50], the model uncertainties are reduced by the direct use of F_Q.

Taking all these novel approaches together, a consistent picture of the charge form factor of the neutron is starting to arise (see fig. 11). Results obtained with different targets and in different reactions are in fair agreement with each other even though at low Q^2 substantial corrections due to rescattering are unavoidable. The data roughly follow a phenomenological parametrisation given by Galster *et al.* already in 1971 [49]. However, the accuracy is reaching a level at which deviations from such a simple, smooth behavior start to become significant [63].

5 Interpretation

With modern experimental techniques, for the first time all elastic nucleon form factors, including the neutron charge form factor, have been measured precisely over a finite range in momentum transfer.

Both magnetic form factors, $G_{M,p}$ and $G_{M,n}$, follow the dipole approximation within 10% up to $Q^2 = 5$ (GeV$/c)^2$. The scaling relation (eq. (4)) is violated considerably for the proton electric form factor. The almost linear decrease of the ratio $G_{E,p}/G_{M,p}$ at $Q^2 > 1$ (GeV$/c)^2$, as revealed by spin transfer measurements at JLab, indicates that the charge density of the proton is significantly softer than its magnetisation density.

Friedrich and Walcher emphasised local deviations from a smooth shape in the Q^2 dependence of all four form factors. By fitting the available data with an ansatz given by the sum of a Gaussian and two dipoles discribing the smooth part, local minima in $G_{E,p}, G_{M,p}$ and $G_{M,n}$ around $Q^2 = 0.25$ (GeV$/c)^2$ with a width of approximately 0.2 (GeV$/c)^2$ as well as a corresponding bump in $G_{E,n}$ are clearly revealed [63].

Nonrelativistically, if the Compton wavelength of a system is negligible compared to its size $\lambda_C = \hbar/Mc \ll \sqrt{\langle r^2\rangle}$, form factors can be measured over a sufficiently large range in momentum transfer in order to calculate spatial densities by a Fourier transform without relativistic effects becoming important. This is the case for atomic nuclei and detailed information about nuclear charge distributions has been obtained from electron scattering [67]. Presently, also the extraction of mass or neutron densities are discussed [68,69].

Although for nucleons $\lambda_C \approx 0.25\sqrt{\langle r^2\rangle}$, a similar interpretation of $G_E(Q^2)$ and $G_M(Q^2)$ as momentum representations of spatial charge and magnetisation densities is still possible in the Breit frame of vanishing energy transfer. Figure 12 shows the corresponding charge distribution of the neutron as calculated by Friedrich and Walcher from their fits.

In coordinate space, the structures observed around $Q^2 = 0.25$ (GeV$/c)^2$ influence the long distance tail ($r \sim 1.5$–2 fm) of charge and magnetisation densities and may be interpreted as resulting from a pion cloud surrounding a bare nucleon. Within this picture, the data for all four form factors can be described by an intuitive phenomenological ansatz consisting of dipole functions for the constituent quarks together with a p-shell harmonic oscillator behaviour of the pion cloud [63].

Another method to analyse and interpret form factors, which does not directly refer to a particular model for nucleon structure, is based on dispersion relations in Q^2. They provide a mathematical framework to connect experimental date in spacelike ($Q^2 > 0$) as well as in timelike ($Q^2 < 0$) regions with spectral functions describing the spectrum of virtual intermediate states, through which a photon can couple to a nucleon [70]. Already early form factor data have been analysed systematically in this framework and it has been established that the spectral functions can be approximated by poles due to the existence of vector mesons and their coupling to nucleons. The prediction of the $\rho(770)$ meson was an early success of this approach [71].

Refined analyses demonstrated the importance of non resonant multi-pion intermediate states [72,73,74]. Two- and tree-pion systems are the lightest possible intermediate states. They provide a link to pion-nucleon scattering and to model-independent predictions from chiral perturbation theory. The analysis method based on dispersion relations as well as the influence of recent data on the spectral functions is discussed by H.W. Hammer [75].

6 Conclusions

In facilities like the Mainz Microtron MAMI, high intensity, polarised, continuous electron beams in the energy range relevant to study phenomena at hadronic scales are available and can be combined with polarised targets and sophisticated detector systems for coincidence experiments and polarimetry.

Electromagnetic form factors are significant observables, directly related to the spatial structure of the nucleon. For the first time, all four nucleon form factors have been measured with a precision sufficient to identify local structures in the Q^2 dependence at a few percent level.

In the near future, measurements of $G_{E,p}/G_{M,p}$ and $G_{E,n}$ will be extended to higher values of Q^2 at Jefferson Lab. Below $Q^2 = 2\ (\mathrm{GeV}/c)^2$, new $^3\overrightarrow{\mathrm{H}}\mathrm{e}(\overrightarrow{e}, e'n)$ as well as absolute $p(e, e')$ cross section measurements are planned at MAMI [76,77].

Besides electromagnetic form factors, a deeper understanding of the elastic nucleon response also includes the weak vector and axial-vector currents. The nucleon axial form factor at low Q^2 has recently been measured in pion electroproduction at MAMI [78] and present-day experiments in parity-violating electron scattering provide access to the two weak vector form factors, which will allow a flavour decomposition of the charge and magnetisation distributions in the nucleon [34,69].

Also beyond elastic scattering, the experimental techniques discussed above help to fully exploit the properties of electromagnetic probes for studies of the much poorer known structure and dynamics of resonances in inelastic processes [79,80].

I would like to thank the organisers of the symposium *20 Years of Physics at the Mainz Microtron MAMI*, Hartmut Arenhövel, Hartmut Backe, Dieter Drechsel, Jörg Friedrich, Karl-Heinz Kaiser and Thomas Walcher and express all the best wishes for the future.

References

1. E.M. Lyman, A.O. Hanson, M.B. Scott, Phys. Rev. **84**, 626 (1951).
2. R. Hofstadter, R.W. McAllister, Phys. Rev. **98**, 217 (1955).
3. G.G. Simon *et al.*, Nucl. Phys. A **333**, 381 (1980).
4. L. Andivahis *et al.*, Phys. Rev. D **50**, 5491 (1994).
5. C.E. Hyde-Wright, K. de Jager, Annu. Rev. Nucl. Part. Sci. **54**, 217 (2004).
6. H.F. Ehrenberg, R. Hofstadter, Phys. Rev. **110**, 544 (1958).
7. A. Lung *et al.*, Phys. Rev. Lett. **70**, 718 (1993).
8. P. Markowitz *et al.*, Phys. Rev. C **48**, R5 (1993).
9. W. Fabian, H. Arenhövel, Nucl. Phys. A **314**, 253 (1979).
10. M. Schwamb, these proceedings.
11. H. Anklin *et al.*, Phys. Lett. B **336**, 313 (1994).
12. E.E.W. Bruins *et al.*, Phys. Rev. Lett. **75**, 21 (1995).
13. H. Anklin *et al.*, Phys. Lett. B **428**, 248 (1998).
14. G. Kubon *et al.*, Phys. Lett. B **524**, 26 (2002).
15. K.I. Blomqvist *et al.*, Nucl. Instrum. Methods A **403**, 263 (1998).
16. J. Arnold *et al.*, Nucl. Instrum. Methods A **386**, 211 (1997).
17. J. Jourdan, I. Sick, J. Zhao, Phys. Rev. Lett. **79**, 5186 (1997).
18. E.E.W. Bruins *et al.*, Phys. Rev. Lett. **79**, 5187 (1997).
19. H. Gao *et al.*, Phys. Rev. C **50**, R546 (1994).
20. W. Xu *et al.*, Phys. Rev. Lett. **85**, 2900 (2000).
21. W. Xu *et al.*, Phys. Rev. C **67**, 012201 (2003).
22. W.K. Brooks, J.D. Lachniet, Nucl. Phys. A **755**, 261 (2005).
23. A.I. Akhiezer *et al.*, Sov. Phys. JETP **6**, 588 (1958).
24. N. Dombey, Rev. Mod. Phys. **41**, 236 (1969).
25. R.G. Arnold, C.E. Carlson, F. Gross, Phys. Rev. C **23**, 363 (1981).
26. J. Golak *et al.*, Phys. Rev. C **63**, 034006 (2001).
27. H. Arenhövel *et al.*, Z. Phys. A **331**, 123 (1988).
28. H. Arenhövel *et al.*, Phys. Rev. C **52**, 1232 (1995).
29. K. Aulenbacher *et al.*, Nucl. Instrum. Methods A **391**, 498 (1997).
30. K.H. Steffens *et al.*, Nucl. Instrum. Methods A **325**, 378 (1993).
31. V. Tioukine *et al.*, contribution to *the 8th European Particle Accelerator Conference (EPAC 2002), Paris, France, 3-7 June 2002*.
32. P. Drescher *et al.*, Nucl. Instrum. Methods A **381**, 169 (1996).
33. A. Jankowiak, these proceedings.
34. F. Maas, these proceedings.
35. D. Eyl *et al.*, Z. Phys. A **352**, 211 (1995).
36. B.D. Milbrath *et al.*, Phys. Rev. Lett. **80**, 452 (1998).
37. T. Pospischil *et al.*, Eur. Phys. J. A **12**, 125 (2001).
38. M.K. Jones *et al.*, Phys. Rev. Lett. **84**, 1398 (2000).
39. O. Gayou *et al.*, Phys. Rev. Lett. **88**, 092301 (2002).
40. J. Arrington, Phys. Rev. C **69**, 022201 (2004).
41. I.A. Qattan *et al.*, Phys. Rev. Lett. **94**, 142301 (2005).
42. L.W. Mo, Y.S. Tsai, Rev. Mod. Phys. **41**, 205 (1969).
43. M. Vanderhaeghen, these proceedings.
44. E. Fermi, L. Marshal, Phys. Rev. **72**, 1139 (1947).
45. S. Kopecki *et al.*, Phys. Rev. C **56**, 2229 (1997).
46. Yu.A. Alexandrov *et al.*, Phys. Part. Nucl. **30**, 29 (1999).
47. H. Leeb, C. Teichtmeister, Phys. Rev. C **48**, 1719 (1993).
48. Yu.A. Alexandrov, Phys. Rev. C **49**, 2297 (1994).
49. S. Galster *et al.*, Nucl. Phys. B **32**, 221 (1971).
50. S. Platchkov *et al.*, Nucl. Phys. A **510**, 740 (1990).
51. M. Meyerhoff *et al.*, Phys. Lett. B **327**, 201 (1994).
52. J. Becker *et al.*, Eur. Phys. J. A **6**, 329 (1999).
53. M. Ostrick *et al.*, Phys. Rev. Lett. **83**, 276 (1999).
54. C. Herberg *et al.*, Eur. Phys. J. A **5**, 131 (1999).
55. D. Rohe *et al.*, Phys. Rev. Lett. **83**, 4257 (1999).

56. D. Rohe, these proceedings.
57. D.I. Glazier *et al.*, Eur. Phys. J. A **24**, 101 (2005).
58. J. Bermuth *et al.*, Phys. Lett. B **564**, 199 (2003).
59. G. Warren *et al.*, Phys. Rev. Lett. **92**, 042301 (2004).
60. R. Madey *et al.*, Phys. Rev. Lett. **91**, 122002 (2003).
61. R. Alarcon *et al.*, contribution to *the 16th International Spin Physics Symposium (SPIN 2004), Trieste, Italy, 10-16 Oct 2004*.
62. R. Schiavilla, I. Sick, Phys. Rev. C **64**, 041002 (2001).
63. J. Friedrich, Th. Walcher, Eur. Phys. J. A **17**, 607 (2003).
64. I. Passchier *et al.*, Phys. Rev. Lett. **82**, 4988 (1999).
65. H. Zhu *et al.*, Phys. Rev. Lett. **87**, 081801 (2001).
66. T. Eden *et al.*, Phys. Rev. C **50**, 1749 (1994).
67. J. Friedrich, N. Voegler, Nucl. Phys. A **373**, 219 (1982).
68. B. Krusche, Eur. Phys. J. A **26**, 7 (2005).
69. S. Kowalski, these proceedings.
70. G. Hohler *et al.*, Nucl. Phys. B **114**, 505 (1976).
71. W.R. Frazer, J.R. Fulco, Phys. Rev. Lett. **2**, 365 (1959).
72. P. Mergell, U.G. Meissner, D. Drechsel, Nucl. Phys. A **596**, 367 (1996).
73. H.W. Hammer, U.G. Meissner, D. Drechsel, Phys. Lett. B **385**, 343 (1996).
74. H.W. Hammer, D. Drechsel, U.G. Meissner, Phys. Lett. B **586**, 291 (2004).
75. H.W. Hammer, these proceedings
76. M.O. Distler (contact person) *et al.*, Experiment MAMI–A1-2/2005.
77. M.O. Distler, W. Heil, D. Rohe (contact persons) *et al.*, Experiment MAMI–A1-1/2005.
78. A. Liesenfeld *et al.*, Phys. Lett. B **468**, 20 (1999).
79. R. Beck, these proceedings.
80. H. Schmieden, these proceedings.